46th AIAA Plasmadynamics and Lasers Conference
22–26 June 2015, Dallas, TX
AIAA-2015-3247

Non-intrusive Velocity and Density Measurements in Subsonic Turbulent Boundary Layer

John M. Sontag[1] and Stanislav Gordeyev[2]
University of Notre Dame, Notre Dame, Indiana, 46556

Aero-optical distortions of a subsonic boundary layer in a spanwise direction were experimentally investigated at different Mach numbers. Convective speeds were extracted as a function of distance from the wall and compared with hot-wire mean velocities. It was found that optically-extracted velocities match hot-wire velocities in the log-region of the boundary layer, suggesting that wavefront sensors can be used to non-intrusively extract the skin friction coefficient using the Clauser method. Aero-optical spectra at different wall-normal distances were also measured and from them characteristic streamwise length scales were estimated. Finally, weighed density fluctuation profiles and the spanwise correlation lengths were measured in wall-normal direction.

I. Introduction

IN the boundary layer of any turbulent flow, the turbulent structures cause density fluctuations which in turn alter the speed of light passing through the region spatially as well as temporally. This issue is generally referred to as the aero-optic problem [1,2] and has been one of the hindrances in furthering our capacity for using lasers on airborne platforms. Understanding the temporal and spatial turbulent fluctuations in a given flow would allow using lasers for high-speed and secure communication across hundreds of miles or as precision targeting systems for military purposes. It also provides a valuable insight into fundamental dynamics and properties of turbulent flows, as information about turbulent structures is "imprinted" onto the laser beam.

The aero-optic problem is a direct result of the relationship between index-of-refraction, n, and density of air, ρ, via the Gladstone-Dale constant, K_{GD} (which is approximately 2.27×10^{-4} m^3/kg in air for visible wavelengths of light) by,

$$n(\bar{x},t)-1=K_{GD}\rho(\bar{x},t) \tag{1}$$

where both index-of-refraction and density are functions of space and time. Unsteady turbulent structures in a flow will vary the index-of-refraction, deflect, distort and scatter the focused laser, and decrease the intensity of the beam at distances far away from the emitting device. To determine the extent to which turbulent density fluctuations effect the propagation of light, an Optical Path Length (OPL) is defined as the integral of the index-of-refraction of a medium along the physical length traversed by a ray of light. Since index-of-refraction and density are related via Equation (1), OPL can be expressed as

[1] Undergraduate Student, Department of Mechanical and Aerospace Engineering, Hessert Laboratory for Aerospace Research, Notre Dame, IN 46556.
[2] Research Associate Professor, Department of Mechanical and Aerospace Engineering, Hessert Laboratory for Aerospace Research, Notre Dame, IN 46556, AIAA Associate Fellow.

$$\mathrm{OPL}(x,y,t)=\int_a^b n(x,y,z,t)dz=\int_a^b\left[K_{GD}\rho(x,y,z,t)+1\right]dz. \quad (2)$$

where z is the direction of beam propagation. The resulting deviation from the space-average OPL can then be expressed as the Optical Path Difference (OPD),

$$\mathrm{OPD}(\vec{x},t)=\mathrm{OPL}(\vec{x},t)-\overline{\mathrm{OPL}(\vec{x},t)}, \quad (3)$$

where the overbar denotes spatial averaging.

Turbulent boundary layers are always present on an airborne platform and affect the outgoing laser beam even in the absence of point-and-track turrets. They are also one of the important fundamental flows with complex dynamics. Aero-optical properties of boundary layers has been extensively studied both experimentally [3 and references therein, 4, 5], and numerically [6].

In all of previous studies the laser beam was propagated through the boundary layer either in a wall-normal direction or close to it, so the aero-optical effects were integrated along the beam, thus losing information about wall-normal variation of various boundary layer properties. In this study, the laser beam was transmitted in a spanwise direction in order to study this wall-normal variation.

Different wavefronts sensors, a Malley Probe and a high-speed wavefront sensor (WFS), were used to measure temporal-spatial variation of aero-optical distortions. As aero-optical distortion convect with turbulent structures, cross-correlating aero-optical aberration between two or more nearby spatial points provides a direct measurement of a convective speed of the structures [3,6,7,8]. By sending the laser beam in the spanwise direction, the flow velocity and density statistics of a turbulent boundary layer as a function of the wall normal distance can be directly and non-intrusively measured. Thus, wavefront sensors can be used as complimentary sensors, which, combined with traditional sensors like hot-wires and PIV, can gain a deeper understanding of the nature of turbulent structures. In this study, simultaneous hot-wire measurements were taken immediately downstream of the Malley Probe beams, for comparison purposes.

For any wavefront sensor, integrated density is essentially the variable that is measured. There are very few other direct methods of obtaining density profiles besides measuring temperature and pressure at every point of interest. One of these is the use of acetone seeding and laser induced fluorescence [9]. This method has been proven to be effective yet carries with it a number of issues regarding calibration. Because of sensitivity to the density field only, any optical-based sensors, including wavefront sensors have a unique potential. Sutton [10] derived a theoretical formulation of a "linking equation" between turbulence quantities and $\mathrm{OPD}_{\mathrm{rms}}$. In a simplified form, it is given as,

$$OPD_{rms}^2 = 2K_{GD}^2 \int_0^L \rho_{rms}^2(s)\Lambda_\rho(s)\,ds, \quad (4)$$

where $\mathrm{OPD}_{\mathrm{rms}}$ is the spatial root-mean square of OPD over an aperture, ρ_{rms} is the root-mean-square density fluctuations, and Λ_ρ is the density correlation length along the beam propagation, s. This equation has been validated both experimentally [3,5] and numerically [6,8]. Typically, the laser beam passes the boundary layer in the wall-normal direction and some estimates should

be made to calculate the density variation along the beam [3,5]. However, by passing the beam in the wall-parallel direction, where the wall-normal direction, y, is constant, both the density fluctuations and the correlation length in the spanwise direction, $\Lambda_Z(y)$, are constant along the beam and Eq. (4) becomes

$$OPD_{rms}^2(y) = 2K_{GD}^2\rho_{rms}^2(y)\Lambda_Z(y)L \tag{5}$$

This allows for direct measurements of the product $\rho_{rms}^2(y)\Lambda_Z(y)$ as a function of the distance from the wall and gaining a further insight into the density structure in turbulent boundary layers.

II. Experimental Setup

The experiments were conducted in the 4″×4″ transonic wind tunnel at the University of Notre Dame's Hessert Laboratory. This facility is an indraft tunnel with an inlet contraction ratio of 150:1, with screens and honeycombs to reduce freestream turbulence intensities. The inlet is followed by a modular smooth wall boundary layer development section, an optical measurement section, and a diffuser, shown schematically in Figure 1.

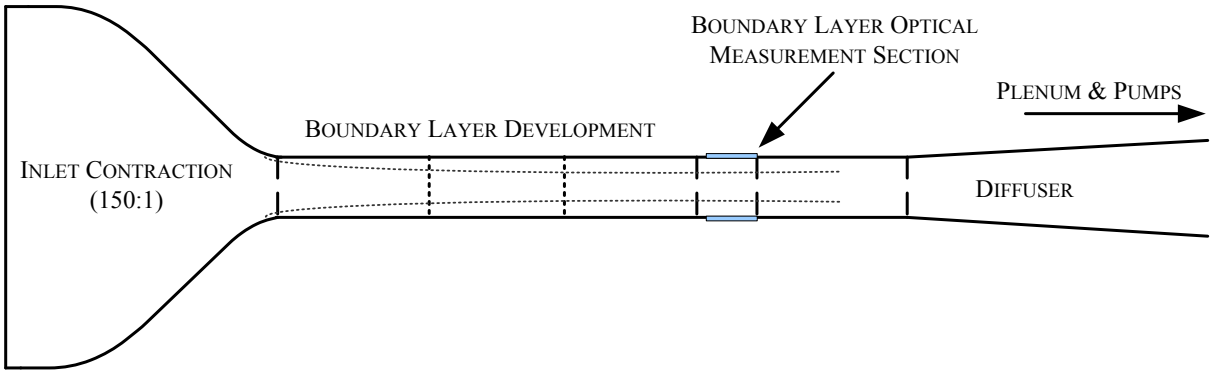

Figure 1. Schematic of the Hessert Laboratory transonic boundary layer wind tunnel, from [3].

The test section is constructed of Plexiglas, with a rectangular cross section that is 10.0 cm in height and 9.9 cm in width. The constant area section of the tunnel can be varied in length to suit different needs. The optical measurement portion of the tunnel was built using optical quality glass instead of Plexiglas to reduce any stationary disturbance imposed on the laser beams. The length of the constant area section in the present study was 116.8 cm. The tunnel velocity is controlled by changing the back pressure in the plenum using vacuum pumps and a pressure bleed valve installed on the plenum. In the Malley-probe/hot-wire study, freestream Mach number was held constant at 0.4. In the Shack-Hartmann WFS study, the same tunnel and test section was used, but freestream Mach number was either 0.5 or 0.6. At the measurement station the boundary layer thickness, δ, was 15.6 mm, the displacement thickness, δ^*, was 2.4 mm, and the momentum thickness, Θ, was found to be 1.74 mm. The Reynolds number based on momentum thickness, Re_Θ, was calculated to be 2.44×10^4 and the shape factor was 1.38.

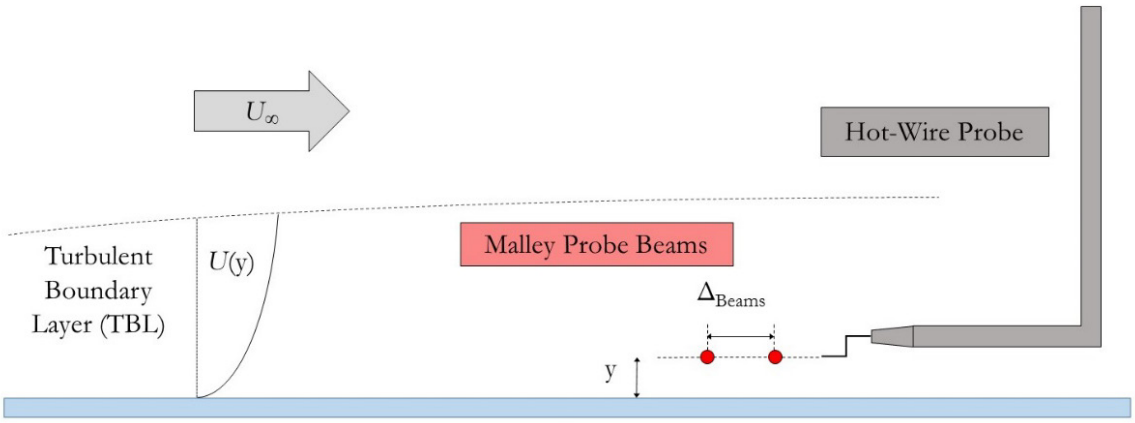

Figure 2. Schematic of experimental Malley-Probe/hot-wire setup, side view.

A Malley Probe was used to collect wavefront measurements in the TBL and a hot wire boundary layer probe was used to collect velocity measurements at a point directly downstream of the Malley Probe beams as shown in Figure 2. In this experiment, the Malley Probe beams were directed along the bottom boundary layer in the spanwise direction through the side walls of the optical measurement section, as shown in Figure 3, left. The streamwise distance between the beams was 6.25 mm. The distance between the Malley Probe beams and the bottom wall was varied by vertically moving the angled steering mirror, see Figure 3, left. This orientation allowed for measurement of convective velocity of the turbulent structures as a function of wall normal direction. The hot wire probe was placed on a separate traverse system and was oriented as close to the downstream beam as possible without inhibiting the beam or inducing flow disturbances at the location of the beam. This was done so that measurements of both devices could be compared with negligible spatial and temporal offset.

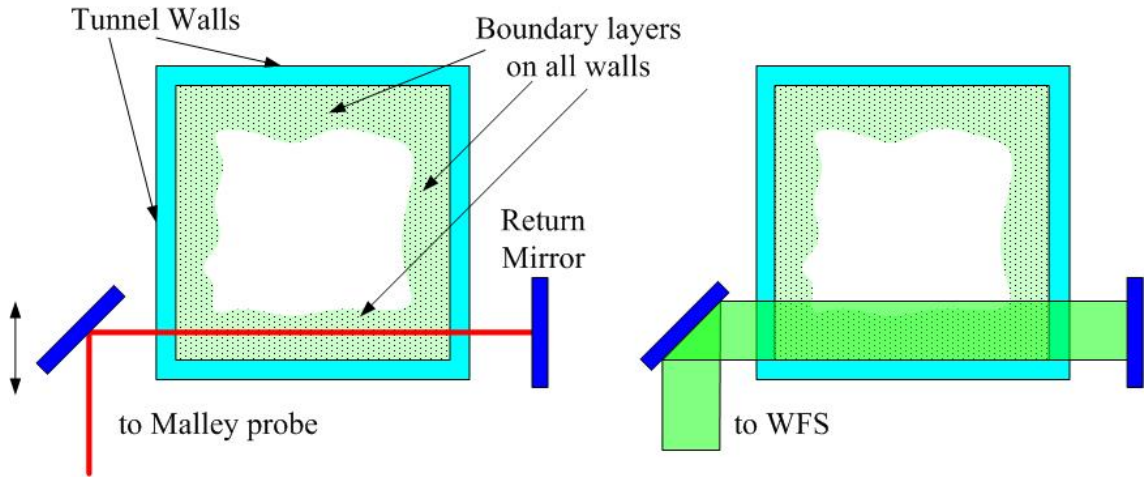

Figure 3. Cross-section view of the beam arrangement for Malley Probe (left) and WFS (right).

The Malley Probe, shown in Figure 4, is a wavefront sensor that measures deflection angle of the two small diameter parallel beams using analog position sensing devices (PSDs) [3]. Using analog PSDs allows for measurements of the time series of deflection angle, $\theta(t)$ at very high sampling frequency (in this case, 200kHz). The Malley Probe was set up to pass through the flow of interest twice in order to increase the signal to noise ratio.

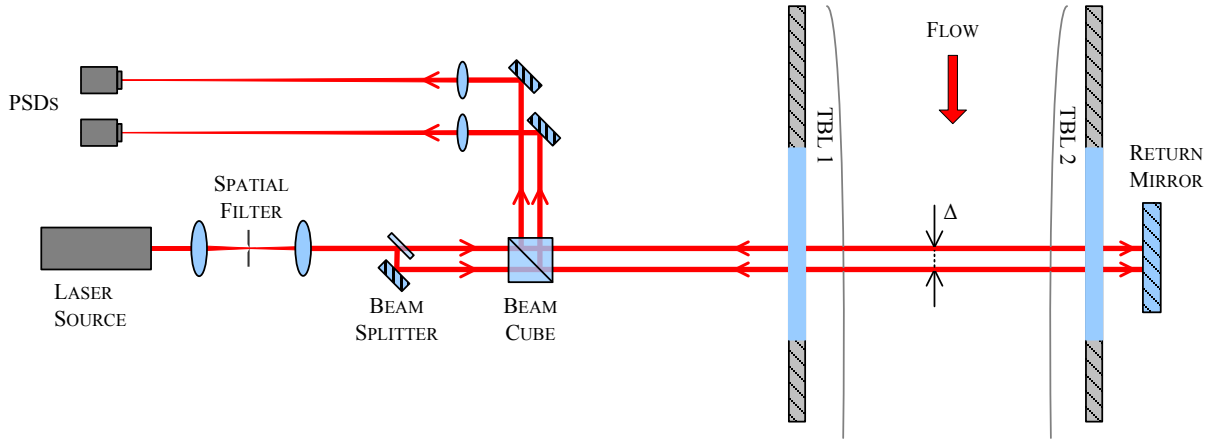

Figure 4. Schematic of a Malley Probe wavefront sensor in a double-pass, double boundary layer measurement configuration, from [3].

From the measured deflection angles, the amplitude spectra, $\hat{\theta}(f)$, were computed for each of the two beams. A critical assumption is made in calculating the convective velocity from $\hat{\theta}(f)$, namely the frozen flow assumption. This assumption allows the deflection angle spectra between two parallel beams, separated by a small distance, Δ, in the flow direction, to be correlated and a convective time delay, τ, between two signals to be calculated. Thus, the convective velocity can be experimentally calculated from the argument or phase of the spectral cross correlation $S(f) = \langle \hat{\vartheta}_1(f)\hat{\vartheta}_2^*(f) \rangle$, where $\hat{\vartheta}_1(f)$ and $\hat{\vartheta}_2(f)$ denote the Fourier transforms of the time series of deflection angle from the first and second beams, respectively, and the star denotes the complex conjugate [3]. Knowing the phase slope, the convective speed can be robustly calculated as $U_c = \Delta/\tau$, where the time delay τ is computed from the slope of the argument, $dArg[S(f)]/df = 2\pi\tau$.

The hot-wire was calibrated in the range of Mach numbers 0.2 – 0.45, and the data was found to be in good agreement with a standard King's Law Fit [11]. To calibrate the hot-wire, the tunnel was run at known speeds and voltage data were collected. A best fit of the data when plotting voltage versus the known velocity yields the King's Law constants A and B for $n = 0.5$.

The Shack-Hartmann WFS, shown in Figure 5, uses the 2-dimensional beam (instead of two small beams for the Malley Probe) to interrogate the flow. The laser beam was expanded to a 25-mm beam and forwarded through the bottom boundary layer in the spanwise direction, as shown in Figure 3, right. After being reflected back by the return mirror along the same way it came and increasing the signal by a factor of two, the returned beam was split off and forwarded onto the high-speed camera Phantom v1610. The camera had a 38 mm focal length, 70 x 60 lenslet array attached, which splits the incoming beam into rectangular array of smaller beams and focuses

each of them onto the sensor, as shown in Figure 6. Knowing the instantaneous dot position and the focal length of the lenslet array, the temporal deflection angle of each beam can be reconstructed. Thus, this set up is similar to the Malley Probe, but essentially uses multiple parallel beams instead of two beams to interrogate the flow.

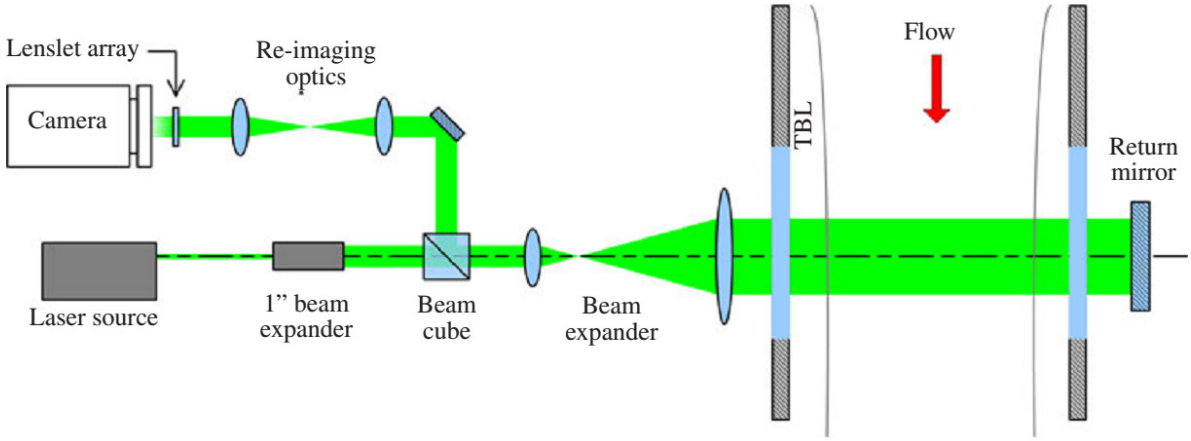

Figure 5. Schematic of a Shack-Hartmann wavefront sensor in a double-pass, double boundary layer measurement configuration, from [3].

To increase the sampling rate of the recorded images, only a small portion of the beam with 4 subapertures in the streamwise direction and 34 subapertures in the vertical direction, extending 20.4 mm away from the bottom wall, were recorded at 250,000 frames per second. These subapertures are outlined with red squares in Figure 6.

In an effort to accurately measure the wall normal distance of the first row of dots, the beam was adjusted in the wall normal direction so that the intensity of the beams along the edge went to zero. Then the beam was moved in the opposite direction until that row was fully visible. Finally the beam was moved back approximately half the distance traversed so that the wall began half of subaperture's size below the first row of beams.

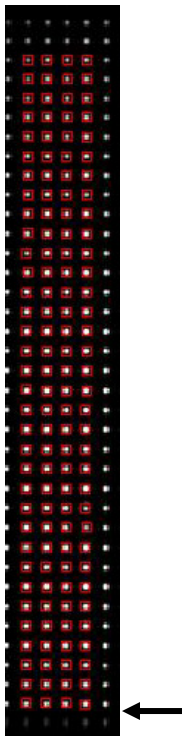

Figure 6. Sample image recorded by the high speed camera in the WFS study. The location of the tunnel wall is indicated by an arrow.

III. Results

Convective velocities were extracted from Malley Probe data using the method described before. As WFS has 4 distinct points in the streamwise direction, it firms 6 unique pairs with a known separation, the same technique as for the Malley Probe data was used to extract convective speeds for each pair. Averaging over these 6 values of convective velocities potentially increases the accuracy of the velocity measurements due to redundancy.

Velocity profiles measured using Malley Probe, hot wire, and WFS data are shown in Figure 7. These profiles show that the convective velocity measured by the Malley Probe agrees with hot-wire results for $y/\delta < 0.2$, then consistently under predicts velocity measured with the hot wire. As the Malley probe measures the convective speed, it does not necessarily coincide with the local mean speed; similar results were observed in supersonic boundary layers [12], where the mean velocity was different from the convective velocity. At $y/\delta = 0.7$ Malley Probe convective speed reaches a peak of approximately $0.9U_\infty$ and then approaches a smaller constant value of $0.85U_\infty$ in the freestream. In the freestream there is no density fluctuation in the flow, so the convective velocity measured in the free stream is due to side-wall boundary layers, schematically shown in Figure 3, left. It is consistent with other measurements of the convective speed of aero-optical structures when the beam is sent normally to the wall [3], where was found the convective velocity to be $0.8\text{-}0.85U_\infty$.

The WFS follows a similar trend as the Malley Probe, see Figure 7, but surprisingly show significant fluctuations in the convective velocity profile, compared to the relatively smooth Malley Probe data. With averaging over 6 distinct beam pairs, it should make the data cleaner than a Malley Probe. Also, below $y/\delta = 0.2$, WFS velocity is higher than either Malley Probe or hot-wire velocities. Comparison of deflection angle spectra at different wall-normal distances, collected with Malley Probe and WFS (not shown) did not reveal any significant differences. Exact reasons for this unexpected discrepancy between Malley Probe and WFS velocities are not quite clear at this point and currently under investigation.

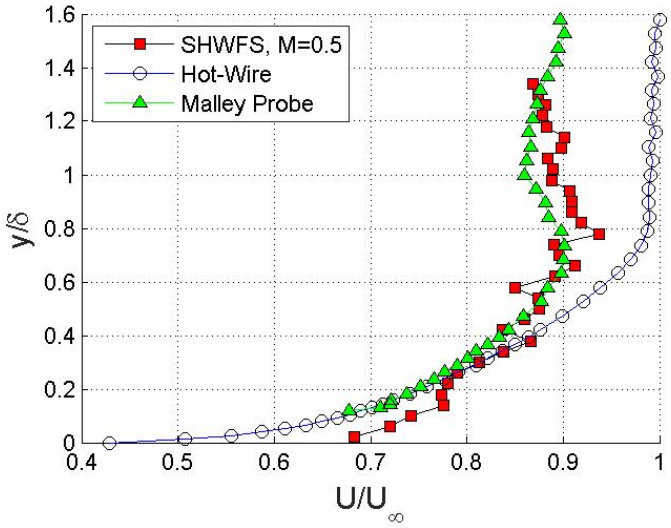

Figure 7. Normalized velocity profiles in outer units for hot-wire, Malley Probe and WFS.

As both hot-wire and Malley Probe velocity agree well near the wall, Malley Probe data might be used to non-intrusively to extract C_f, using the Clauser method. To check it, the same velocity profiles, as in Figure 7, were re-plotted in inner units. The skin friction velocity, u_τ, needed to compute the inner units, was calculated from C_f as $u_\tau = U_\infty \sqrt{C_f/2}$. The skin friction

coefficient, C_f, in turn, was computed from Re_Θ using the second Coles-Fernholz relation with modified constants [13], $C_f = 2[2.604\ln(\mathrm{Re}_\theta) + 4.127]^2$. Figure 8 shows the comparison of the three data sets, along with the theoretical line, $U^+ \equiv U/u_\tau = 1/\kappa \cdot \ln(y^+) + C$. It can be seen that both hot-wire and the Malley Probe velocities follow the theoretical line in the log-region. Thus, Malley Probe sensor can potentially be used to non-intrusively measure velocity in the log-region and extract the skin friction coefficient using the Clauser method.

Due to some amount of uncertainty in the wall normal distance for WFS data, a sensitivity analysis was conducted to determine how much this uncertainty affected the slope of this plot. Even in the extreme case of being off by half of subaperture's size in the wall normal distance, the slope only varied by about 15% and never came close to the slope seen in the other two sets of data. The actual uncertainty in the wall normal distance is far less than half an aperture size and therefore it is concluded that this uncertainty doesn't play a significant part in the discrepancy.

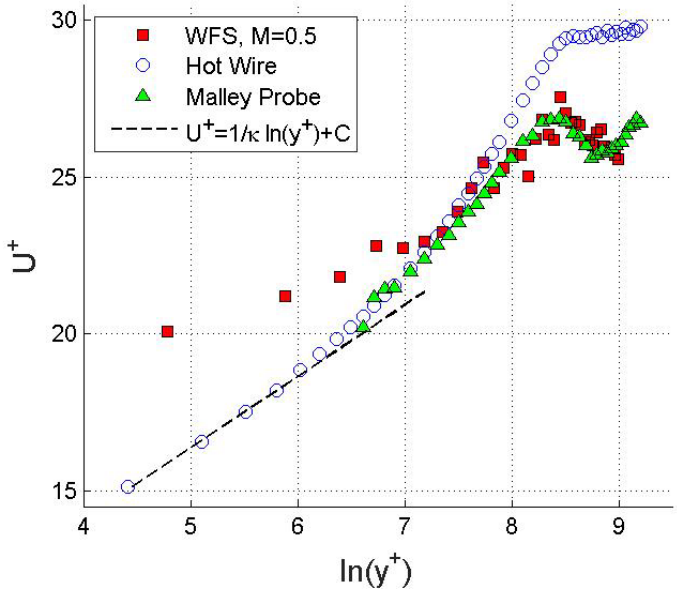

Figure 8. Comparison of hot wire mean velocities, and Malley Probe and Shack-Hartmann convective velocities in inner units.

The deflection angle amplitude spectra at several wall-normal locations are shown in Figure 9. As the deflection angle spectrum is the pre-multiplied amplitude wavefront spectrum [3], the location of the peak indicates the size of the dominant aero-optical structure. As expected, the structure is smaller near the wall, resulting in the spectrum peak around $St_\delta \sim 4$ at $y/\delta = 0.02$. This spectral peak corresponds to the dominant streamwise aero-optical structure with a characteristic length of $L_x \sim U_C / f_{peak} = \frac{U_C}{U_\infty}\frac{U_\infty \delta}{\delta f_{peak}} = \delta \frac{U_C}{U_\infty}\frac{1}{St_\delta} = \delta \cdot 0.5/4 = 0.12\delta$. The peak shifts to $St_\delta = 3$ at $y/\delta = 0.06$ with $L_x \sim 0.2\delta$, reaches $St_\delta = 1$ around $y/\delta = 0.4$ ($L_x \sim 0.8\delta$) and near the edge of the boundary layer approaches $St_\delta \sim 0.8$, corresponding to $L_x \sim 1.2\delta$. Outside the

bottom boundary layer, the spectrum approaches the spectrum due to the independent boundary layers on side walls, with the peak around $St_\delta = 1$ [3].

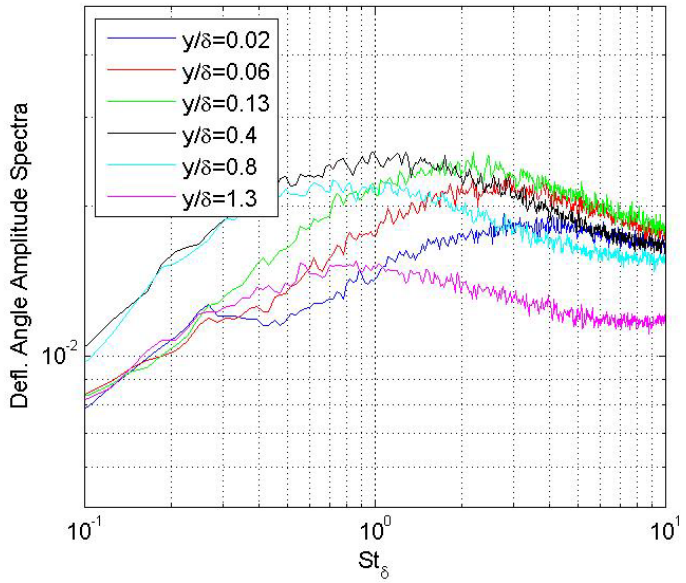

Figure 9. WFS deflection angle spectra at various wall normal distances.

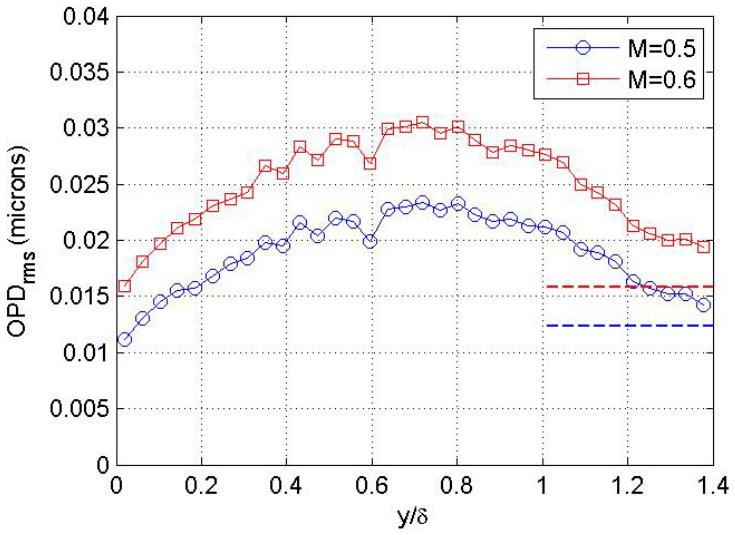

Figure 10. OPD_{rms} profiles across the boundary layer for M = 0.5 and 0.6.

Deflection angle spectra at each wall-normal location were integrated to obtain aero-optical distortions [3] along the spanwise direction as,

$$OPD_{rms}^2(y) = 2U_C(y)\int_0^\infty \frac{\left|\hat{\theta}(f)\right|^2}{(2\pi f)^2} df$$

Wall-normal distributions of the OPD_{rms} for both M = 0.5 and M = 0.6 experiments are shown in Figure 10. M=0.6 is consistently higher then M=0.5 case, as aero-optical distortions in subsonic boundary layers are proportional to M^2 [3]. OPD_{rms} are low near the wall, reach a maximum

approximately around $y/\delta = 0.7$ and decrease in the outer part of the boundary layer. If only a bottom boundary layer is present in the test section, OPD_{rms} would approach a zero value. Instead, OPD_{rms} reaches a constant value outside the boundary layer, as the laser beam starts traversing through the two side-wall boundary layers. Knowing the side-wall boundary layer thickness and the freestream speed, aero-optical distortions due to these boundary layers were computed [3] and results are plotted in Figure 10 as dashed lines for both Mach numbers. Experimental results outside the boundary layer agree well with the expected aero-optical distortions.

The linking equation, Eq. (4), relates the density profile to the aero-optical distortions through the vertical distribution of the spanwise correlation length, $\Lambda_Z(y)$. From OPD_{rms}, density profiles, weighted by $(\Lambda_Z/\delta)^{0.5}$, were computed and results for both Mach numbers are plotted in Figure 11, left. Density fluctuations increase with Mach number, as expected.

Thus, this technique can be used to compare density profiles for boundary layers with the same spanwise correlation length, like adiabatic and moderately cooled-wall boundary layers [5], where it was found that the velocity structure, and therefore all correlation lengths, are unchanged by the cooled wall, while density fields are reduced significantly.

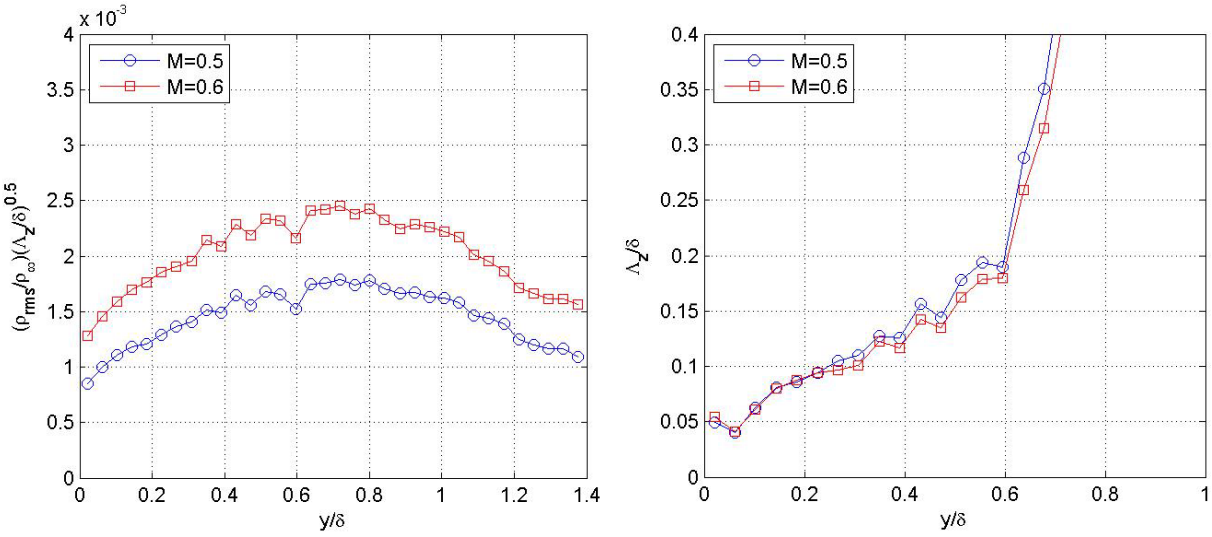

Figure 11. Left: Density fluctuation profiles, weighed by $(\Lambda_Z/\delta)^{0.5}$. Right: Correlation length as a function of wall normal distance.

If the spanwise correlation length is known, the density profile can be calculated non-intrusively. So, the correlation length $\Lambda_Z(y)$ needs to be measured or estimated somehow. In [3,5] it was shown that both adiabatic and non-adiabatic boundary layers the wall-normal density distribution, $\rho_{rms}(y)$, can be accurately estimated from velocity profiles using the Extended Strong Reynolds Analogy. In case of subsonic, adiabatic boundary layers the density profile is

$$\rho_{rms}(y) = \rho_\infty(\gamma-1)rM_\infty^2\sqrt{C_f/2}\,f(y)g(y) + O(M^4), \text{ where}$$

$$f(y) = U(y)/U_\infty,$$

$$g(y) = u_{rms}(y)/u_\tau$$

Here, U and u_{rms} are the mean and fluctuating velocity components, respectively, $\gamma = 1.4$, $r = 0.89$ is the recovery coefficient, C_f is the skin friction coefficient and u_τ is the skin friction velocity. Functions f and g from [5] were used, C_f was estimated from Re_Θ using the second Coles-Fernholz method [13].

Solving the linking equation for the correlation length for both Mach numbers yielded the plot in Figure 11, right. Correlation length increases approximately linearly through the boundary layer up to $y/\delta = 0.6$, with typical values of Λ_Z/δ between 0.1 and 0.2. These values are comparable with the wall-normal correlation lengths estimated from velocity fields [14,15] or computed numerically [6]. The correlation length Λ_Z increases rapidly above $y/\delta = 0.6$, most probably because aero-optical results were contaminated by the presence of the side-wall boundary layers. Additional measurements in the boundary layer with different spanwise widths are needed to accurately measure the spanwise-correlation above $y/\delta = 0.6$.

IV. Conclusions

Experimental measurements of aero-optical distortions in the subsonic boundary layer along the spanwise direction were presented and discussed. Two different wavefront sensors, Malley probe and a Shack-Hartmann wavefront sensor, were used to record temporal sequences of deflection angles imposed on laser beams. By cross-correlating time series of beams spaced in a streamwise direction, convective speeds of aero-optical structures were extracted at different distances from the wall. Comparison of convective speeds with mean velocity profiles, obtained with a hot-wire, reveal that the Malley Probe provides correct velocity values inside the log-region of the boundary layer. The convective speeds in the outer portion of the boundary layer were found to be consistently less than the mean velocity values. Plotted in inner units, velocities collected with the Malley Probe and hot-wire, collapse with the theoretical prediction of the velocity profile in the log-region. So, the wavefront sensors like the Malley Probe can be potentially used to measure the velocities inside the log-region and non-intrusively estimate the skin friction coefficient, using the Clauser method.

Analysis of the deflection angle spectra at different distances from the wall gave a qualitative estimate of the streamwise characteristic size of aero-optical structures, as well as levels of aero-optical distortions at different wall-normal locations. Using the linking equation, weighted density fluctuation profiles were extracted. Finally, using the Strong Reynolds Analogy, the velocity spanwise correlation length was found as a function of wall normal distance.

These preliminary experiments undoubtedly show that these non-intrusive wavefront sensors could be used as valuable complimentary sensors in measuring the properties of velocity and density structures in turbulent flows. One obvious limitation of this non-intrusive measurement technique is that it calculates the velocity and density properties averaged along the laser beam, thus limiting flows of interest to spanwise-uniform flows. However, the non-intrusive nature of the technique might be very useful in conducting measurements at high supersonic and hypersonic speeds, where there are many difficulties of using intrusive-type sensors. Another

application of this technique is in flows which are very sensitive to any intrusive sensors, like the transitional flows.

Acknowledgements

The authors would like to acknowledge Adam Smith for helping set up the experiments and for valuable suggestions in reducing the data.

References

[1] Jumper, E.J., and Fitzgerald, E.J., "Recent Advances in Aero-Optics," *Progress in Aerospace Sciences,* **37**, pp. 299-339, 2001

[2] Wang, M., Mani, A., and Gordeyev, S., "Physics and Computation of Aero-Optics", *Annual Review of Fluid Mechanics*, **44**, pp. 299-321, 2012.

[3] S. Gordeyev, A.E. Smith, J.A. Cress and E.J. Jumper. Experimental studies of aero-optical properties of subsonic turbulent boundary layers. *Journal of Fluid Mechanics*, *740*, pp 214-253, 2014.

[4] S.Gordeyev, E. Jumper and T. Hayden, "Aero-Optical Effects of Supersonic Boundary Layers," *AIAA Journal*, **50**(*3*), pp. 682-690, 2012.

[5] S. Gordeyev, J.A. Cress, A Smith and E.J. Jumper, "Aero-optical measurements in a subsonic, turbulent boundary layer with non-adiabatic walls", *Physics of Fluids*, **27**, 045110, 2015.

[6] Wang, K. and Wang, M., "Aero-optics of subsonic turbulent boundary layers," *Journal of Fluid Mechanics*, **696**, pp 122-151, 2013.

[7] A.E. Smith, S. Gordeyev, H. Ahmed, A. Ahmed, D.J. Wittich III and M. Paul, " Shack-Hartmann Wavefront Measurements of Supersonic Turbulent Boundary Layers in the TGF ", AIAA Paper 2014-2493, 2104.

[8] Wang, K. and Wang, M., "On the accuracy of Malley probe measurements of aero-optical effects: a numerical investigation," *J. Opt. Eng.* **52**(*7*), 071407, 2013.

[9] Reid, J.Z., Lynch, K.P. and Thurow, B.S., "Density Measurements of a Turbulent Wake Using Acetone Planar Laser-Induced Fluorescence," *AIAA Journal,* **51**(*4*), pp. 829-839, 2013.

[10] Sutton, G.W., "Effect of Turbulent Fluctuations in an Optically Active Fluid Medium," *AIAA Journal* **7**(*9*), pp. 1737-1743, 1969.

[11] King, L. V. 1914 On the convection of heat from small cylinders in a stream of fluid, with applications to hotwire anemometry. *Phil. Trans. R. Soc.* 211 373332.

[12] Spina, E.F., Donovan, J.F and Smits, A.J. "Convection velocity in supersonic turbulent boundary layers," Phys. Fluids A **3**(*12*), pp. 3124-3126, 1991.

[13] Nagib, H.M., Chauhan K.A. & Monkewitz P.A., "Approach to an asymptotic state for zero pressure gradient turbulent boundary layers," *Phil. Trans. R. Soc. A* **365**, pp. 755-770, 2007.

[14] Gilbert, K.G., "KC-135 Aero-Optical Boundary-Layer/Shear-Layer Experiments," Aero-Optical Phenomena, Eds. K.G. Gilbert and L.J. Otten, Vol. 80, Progress in Astronautics and Aeronautics, (AIAA, New York, 1982), 306-324.

[15] Rose, W.C., "Measurements of Aerodynamic Parameters Affecting Optical Performance," Air Force Weapons Laboratory Final Report, AFWRL-TR-78-191 (1979).